Jiang, L.; Gerkema, T.; Wijsman, J.W.M. & Soetaert, K. (2019). Comparing physical and biological impacts on seston renewal in a tidal bay with extensive shellfish culture. *Journal of Marine Systems*, 194, 102-110

Comparing physical and biological impacts on seston renewal in a tidal bay with extensive shellfish culture

Long Jiang[1], Theo Gerkema[1], Jeroen W.M. Wijsman[2], Karline Soetaert[1]

[1]Department of Estuarine and Delta Systems, Royal Netherlands Institute for Sea Research (NIOZ) and Utrecht University, P.O. Box 140, 4400 AC Yerseke, The Netherlands.

[2]Wageningen Marine Research, Wageningen University and Research, P.O. Box 77, 4400 AB Yerseke, The Netherlands.

Corresponding author: L. Jiang (long.jiang@nioz.nl)

Highlights:

- Landward seston depletion induced by bivalve filtration in a Dutch coastal bay
- Comparable biological and physical impacts on the seston dynamics
- A straightforward approach useful for shellfish culture management

Formatted for *Journal of Marine Systems* (March 2019)

Abstract

Shellfish cultures worldwide are often located in sheltered marine bays. The Oosterschelde is such a bay in the southwestern delta of the Netherlands, harboring extensive shellfish cultures, whose yield is partly driven by seston renewal from the North Sea. Tracer experiments performed with a three-dimensional hydrodynamic model were used to study the relative influences of benthic filtration and physical processes on seston replenishment. The model exhibited good skills in reproducing observed water level, temperature, salinity, and current velocity during 2009–2010. Turnover and residence times as indicators of water renewal showed substantial gradients from the mouth to head of the Oosterschelde. Surveyed bivalve biomass and empirical filtration rates were incorporated to estimate the effects of aquaculture on the seston concentration. The filtration created strong bio-deposition suppressing the eastward seston transport and causing less than 10% of external seston to be delivered to the head of the Oosterschelde. The effect of biological filtration on seston transport was comparable to that of physical forcing. This simple approach combining effects of physics and benthic communities can be applied more generally in food sustainability assessments of tidal bays.

Keywords

Tidal bay; suspension feeders; seston transport; tracer experiment; turnover time; residence time

1. Introduction

Due to logistic constraints, shellfish cultures throughout the world are often located in sheltered marine bays that are productive, easily accessible, and not so vulnerable to extreme weather conditions (Heip et al., 1995; Filgueira et al., 2015). In tidal bays with limited freshwater discharge compared to the tidal prism, tidal-induced water renewal with the adjacent coastal sea drives the exchange of dissolved and particulate matters, which is critical to water quality and ecosystem functions including shellfish production (Boynton et al., 1995; Filgueira et al., 2014; Jouon et al., 2006; Spillman et al., 2008). As suspension feeder biomass is found to be significantly affected by the water renewal efficiency (Heip et al., 1995), water renewal time has been extensively applied for aquaculture carrying capacity assessments (Gibbs et al., 2007; Grant & Filgueira, 2011; Spillman et al., 2008). Typically, such an assessment is conducted on a system-wide scale, by comparing renewal timescales, such as residence time (*RT*) and clearance time (*CT*), the time for suspension feeders to filter the total volume of water (Dame & Prins, 1997; Heip et al., 1995; Smaal & van Duren, 2019). The ratio *CT*/*RT* well below one points to overexploitation, whereas ecosystems with *CT*/*RT* above 20 are considered sustainable (Filgueira et al., 2015).

Whereas these basin-wide carrying capacity assessments have been successfully applied, the strong filtration induced by shellfish also modulates the spatial distribution of phytoplankton and other particulate organic matter (POM) and affects their replenishment (Grangeré et al., 2010; Guyondet et al., 2013). Generally, seston distribution and renewal are thought to be predominately driven by hydrodynamic conditions in estuaries worldwide ranging from Chesapeake Bay (North et al., 2004) to smaller ones (Carter, 1976; Chaparro et al., 2008; Moser et al., 2005). However, if biological sources/sinks are strong enough, the physics-driven renewal processes of solutes and particles may be substantially changed. For instance, in a tidal basin where the coastal sea is the dominant seston source, strong biological seston consumption near the entrance may reduce the replenished seston far away from the entrance. Similarly, a non-negligible biological source of solutes or particulates in such a basin can make the substance concentration higher compared to that calculated from tidal

renewal alone. Yet, the estimation of shellfish food availability is often only based on physical residence time (Guyondet et al., 2005; Koutitonsky et al., 2004), with limited studies on the combined impacts of physics and biology (e.g., benthic filtration).

The Oosterschelde is a tidal bay on the southwest coast of the Netherlands (Figure 1a). Since the construction of a semi-open storm surge barrier at its mouth and the compartmentalization dams and sluices in the late 1980s, the system gradually evolved from an estuary into a tidal bay, where tides dominate the water exchange (Nienhuis & Smaal, 1994; Ysebaert et al., 2016). The Oosterschelde harbors an intensive benthic bivalve aquaculture, predominantly mussels, and is heavily exploited. While the post-barrier *RT* ranges 20–135 days from west to east (Dame & Prins, 1997), cultured and wild suspension feeders can filter the water column in around ten days (Smaal et al., 2013). The low *CT*/*RT* ratio (< 1) indicates the bivalve standing stocks exceeding the sustainable limits and implies a relatively strong biological seston sink in the Oosterschelde, which makes it a suitable system to compare the biological and physical effects on seston dynamics.

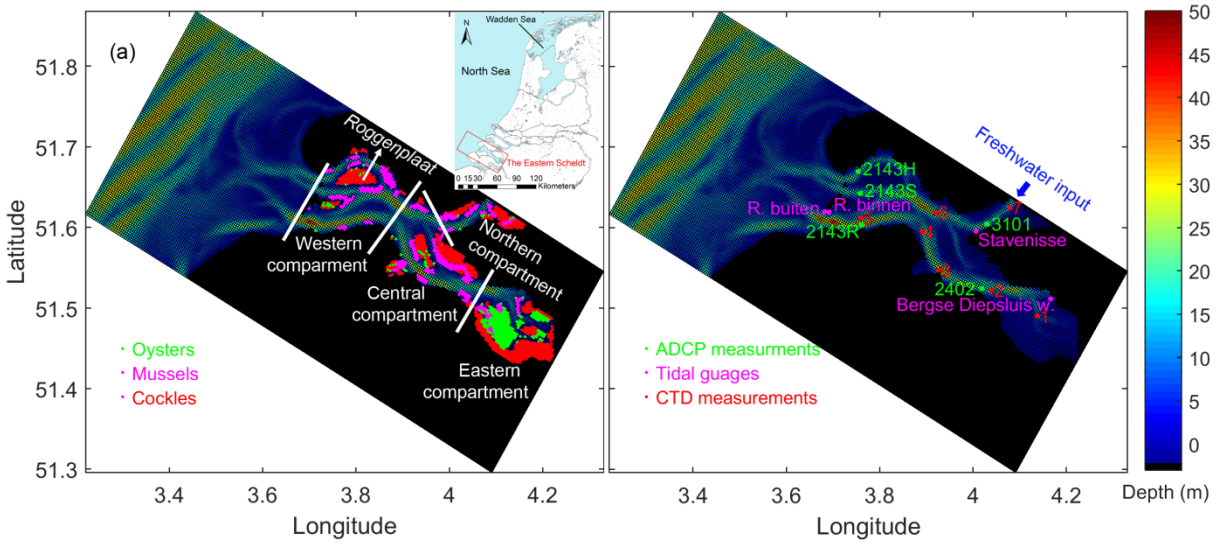

Figure 1. The model domain, grid, and bathymetry of the Oosterschelde with (a) the mapped distribution of three suspension feeders examined in this study (mussels, cockles, and oysters) and (b) the locations of the river boundary and data (temperature, salinity, water elevation, and current velocity) sites for model calibration and validation. The white lines in (a) denote the theoretical boundaries of four compartments. The inset in (a) shows the geographical location in a larger map of the Netherlands.

Phytoplankton and other POM constitute the predominant food for shellfish, and bivalve grazing is assumed to have led to declining primary production in the Oosterschelde (Smaal et al., 2013). Grazing causes significantly lower seston concentrations during ebb compared to flood tides (Prins et al., 1996; Smaal & van Stralen, 1990; van Stralen & Dijkema, 1994), indicating that seston import from the North Sea provides a substantial source of food for the bivalve culture. This is evidenced by higher growth rates and meat content of cultured mussels in the well-flushed western compartment (Figure 1b). Whereas it is generally claimed that the yield of culture plots in the Oosterschelde is controlled by the seston transport driven by hydrodynamic conditions (van Stralen & Dijkema, 1994), the extent to which this is affected by the shellfish themselves has not yet been assessed.

In this study, a tracer was implemented in a three-dimensional hydrodynamic model to study seston dynamics in the Oosterschelde. We added a simple benthic module to test how seston distribution is impacted by the extensive benthic filtration. We examine how important biological forces (filtration) are in comparison with physical forces in the system and how this varies spatially. We believe that our model used here may aid to optimize spatial distribution of culture plots so as to efficiently utilize available food resources.

2. The study site

The Oosterschelde is a 350-km^2 tidal bay (tidal range 2.9–3.5 m) with deep channels (up to 50 m deep), flanking shoals, and extensive tidal flats (110 km^2). It is typically divided into four compartments, the western, central, eastern, and northern (Figure 1a). Freshwater runoff entering the northern compartment is slightly below 10 $m^3\ s^{-1}$ (Figure 1b, Ysebaert et al., 2016). The storm surge barrier built in the 1980s reduced the cross-sectional area of the mouth opening by 78% and the tidal prism and velocity by ~30%, which caused the ongoing erosion of tidal flats and deposition in channels (Nienhuis & Smaal, 1994). The water column is mostly well mixed with salinity ranging 30–33 (Wetsteyn & Kromkamp, 1994). Seaward increasing salinity, Chl-a, and turbidity are observed owing to influences from the North Sea (Nienhuis & Smaal, 1994; Wetsteyn & Kromkamp, 1994).

Table 1

The surveyed bivalve biomass (kilotons fresh weight) in the Oosterschelde in the year 2009 (Source: Wageningen Marine Research).

Species	Scientific name	Eastern	Central	Western	Northern
Cockles	*Cerastoderma edule*	4.62	13.64	13.97	8.41
Blue mussels (wild)	*Mytilus edulis*	0.22	0.00	0.00	0.23
Blue mussels (cultured)	*Mytilus edulis*	0.00	11.23	18.89	2.98
Pacific oysters (wild)	*Crassostrea gigas*	13.89	9.97	8.66	10.67
Pacific oysters (cultured)	*Crassostrea gigas*	6.71	0.00	0.00	0.00
Baltic clams	*Limecola balthica*	0.03	0.07	0.16	0.02
Manila clams	*Venerupis philippinarum*	0.30	0.00	0.00	0.00
Razor clams	*Ensis leei*	0.22	0.05	8.14	0.91
Soft-shell clams	*Mya arenaria*	0.01	0.01	0.01	0.01

Benthos of the Oosterschelde is dominated by bivalve filter feeders including the introduced Pacific oysters (*Crassostrea gigas*), blue mussels (*Mytilus edulis*), and cockles (*Cerastoderma edule*) (Smaal et al., 2009, 2013), accounting for 92.6% of the overall surveyed shellfish biomass in 2009 (Table 1). Cockles and most Pacific oysters are mainly wild stocks distributed on tidal flats, while aquaculture contributes most to the mussel biomass in the Oosterschelde (Table 1). Most productive mussel culture plots are in the western and central compartments, and oysters are mainly cultured in the eastern compartment (Figure 1a and Table 1). In recent decades, the cockle biomass has been subject to natural fluctuations due to changing environmental conditions; the mussel stocks are under anthropogenic control depending on the abundance of seeds; the invasive Pacific oyster population expanded before the late 2000s and has decreased due to increasing fishing pressure since then (Smaal et al., 2013). The overall shellfish population has been stable in the past decade, producing 20–40 and 3 kilotons fresh weight of cultured mussels and oysters per year, respectively (Wijsman et al., 2019). Additionally, the presence of bivalves makes the

Oosterschelde an international nature conservation area for wader birds (Tangelder et al., 2012).

3. Methods

3.1. Model description

The open-source General Estuarine Transport Model (GETM, https://getm.eu) was applied in this study to simulate the circulation and transport in the Oosterschelde. GETM is a widely used hydrodynamic model designed for estuaries and coastal oceans. It solves the hydrostatic momentum, salinity, temperature, density, and continuity equations with a module to simulate the periodic drying of tidal flats and is combined with the General Ocean Turbulence Model (GOTM, http://gotm.net), governing the vertical turbulence closure schemes. Prior applications of GETM (e.g., Burchard et al., 2004; Duran-Matute et al., 2014; Mohrholz et al., 2015) and its user manual include detailed formulations of this model.

In our model set-up, GETM was run on a 300 m × 300 m Cartesian grid covering the Oosterschelde and the adjacent part of the North Sea (Figure 1). Ten equidistant terrain-following layers were applied vertically. The third-order TVD-P2-PDM and second-order TVD-SUPERBEE were used as horizontal and vertical momentum schemes, respectively. The model was run for years 2009–2010. The bathymetry data is regularly measured by the Dutch government agency Rijkswaterstaat (accessible from http://opendap.deltares.nl). We selected the bathymetry data that are measured closest to the model period, which was then interpolated and smoothed following the method of Duran-Matute et al. (2014). Specifically, the bathymetry used inside the Oosterschelde was derived from the year 2007.

The hydrodynamic model was forced with tides, freshwater discharge, and meteorological forcing. Tidal transport and height at the open boundary were interpolated from the Northwest European Shelf tidal prediction and assimilation by Oregon State University (Egbert et al., 2010). Remote wind surges were not prescribed at the open boundary, but local winds within the domain were included via atmospheric forcing. Open-boundary temperature and salinity were extracted from a GETM-based North Sea model with a resolution of 5 km (van der Molen et al., 2016). Freshwater discharge from sluices into the northern branch was obtained from Ysebaert et al. (2016). Atmospheric forcing including hourly mean winds, air pressure, air temperature, precipitation, and humidity was provided by a downscaled weather forecasting model HARMONIE with a horizontal grid of 2.5 km produced by the Royal Dutch Meteorological Institute (KNMI).

During the 2-year simulation period, the model was calibrated and validated with observed water level, temperature, salinity, and current velocity. Water level data every ten minutes at tidal gauges were acquired from Rijkswaterstaat. Monthly or biweekly temperature, salinity, and near-surface (~5 m) suspended particulate matter (SPM) data were measured at various tide conditions (slacks, flood, and ebb) by the NIOZ (Royal Netherlands Institute for Sea Research) as part of an annual monitoring program. Current velocity data within one full tidal cycle (12–13 hours) were collected by Rijkswaterstaat at different times and locations in 2010. All these measurement stations are indicated in Figure 1b.

3.2. Tracer experiments and renewal timescales

Eulerian passive tracer experiments are widely applied in estimating renewal timescales (Luff & Pohlmann, 1995). The governing equation for tracer concentration in GETM is as follows.

$$\frac{\partial C}{\partial t} + u\frac{\partial C}{\partial x} + v\frac{\partial C}{\partial y} + w\frac{\partial C}{\partial z} - K\frac{\partial}{\partial z}\left(\frac{\partial C}{\partial z}\right) - F_h = 0 \quad (1)$$

In Equation (1), C is the tracer concentration (unitless); x, y, and z are the three-dimensional spatial coordinates within the model (m); u, v, and w are the velocity in the x, y, and z directions (m s^{-1}), respectively; K is the vertical turbulence diffusivity calculated from GOTM (m^2 s^{-1}), used in temperature and salinity calculation as well; and F_h is the horizontal diffusion term (concentration s^{-1}). Generally, tracers are placed inside estuaries/lagoons and how concentrations decrease over time is modeled. In our study, the tracer, simulated for 2009, was used as a proxy of the more abundant seston in the North Sea relative to the Oosterschelde, so its concentration was initially set to 1 in the North Sea (C_{NS}) and 0 for the Oosterschelde. Calculations of renewal timescales were adjusted correspondingly.

We estimated the turnover time (TT), which is widely used in environmental assessments for aquaculture. It is defined as the time when $1 - 1/e$ (~63.2%) of the initial amount of tracer mass in the embayment is replaced with seawater (Guyondet et al., 2005; Koutitonsky et al., 2004; Zimmerman, 1976), based on the assumption that the embayment water decreases exponentially in time (Aubrey et al., 1993). In our application, the fraction of original water without tracers equals $(C_{NS} - C_t)/C_{NS}$, where C_t is the local tracer concentration at any time t. Based on the definition of TT, this fraction follows the relationship $(C_{NS} - C_t)/C_{NS} = exp(-t/TT)$. This allows to estimate TT at any point. The time series of C_t at all grid cells went through a low-pass filter with a threshold frequency 1/48 h (Flagg et al. 1976), and TT was designated as the last time when C_t exceeded $(1 - e^{-1}) \cdot C_{NS}$.

Given the possible violations of the exponential assumption (Monsen et al., 2002), we also RT calculated using the remnant function approach (Takeoka, 1984). Time series of spatial tracer concentrations was used for the RT calculation as follows:

$$RT = \int_0^\infty \frac{C_{NS} - C_t}{C_{NS}} dt \quad (2)$$

Since in the definitions it will take infinite time for the tracer concentration inside the bay to reach C_{NS}, the upper limit of the integration time was specified as 365 days, the length of the model run. If the exponential assumption of tracer concentration holds, the two timescales are equivalent by definition (Takeoka, 1984).

3.3. Implementation of suspension feeders in the model

Impacts of the three dominant suspension feeders, mussels, cockles, and oysters, were simulated by combining measured standing stocks with individual filtration rates. Table 1 shows the surveyed biomass of the Oosterschelde in the simulation year 2009 (Smaal et al., 2013). The standing stocks of these three species (fresh weight, g) were converted to tissue dry weight (DW, g) using the empirical factors of 0.066 for mussels, 0.03 for cockles, and 0.02 for oysters according to Wijsman and Smaal (2017). Number of individuals in all cells N was estimated as DW/W, where W is the median dry weight per individual based on the Wageningen Marine Research (WMR) sampling campaigns of the Oosterschelde, 1.5 g for mussels, 2 g for oysters, and 1 g for cockles. The DW-based individual net filtration rates (F, L hr^{-1}) were derived based on multiple measurements (Cranford et al., 2011; Wijsman and Smaal, 2017): for mussels, $F/F_0 = 1.66*(W/W_0)^{0.57}$; for cockles, $F/F_0 = 1.44*(W/W_0)^{0.69}$; for oysters, $F/F_0 = 3.92*(W/W_0)^{0.50}$; where F_0 and W_0 are unit filtration rate 1 L hr^{-1} and DW 1 g, respectively. Based on the spatial mapping of suspension feeders (WMR data, Figure 1a), assuming they are uniformly distributed within grid cells, the integrated filtration rate was estimated as a function of species-specific filtration rates (F_i) and number of individuals (N_i). Given that suspension feeders tend to digest or deposit all the filtered seston (3–100 μm,

Wildish & Kristmanson, 1993), even when exceeding their metabolic needs (Heip et al., 1995), a loss term was added to the tracer in the bottom layer (C_{bottom}) as follows:

$$\frac{dC_{bottom}}{dt} = -C_{bottom} \cdot \frac{\Sigma_{i=1,2,3} F_i N_i}{V_{bottom}}, \quad (3)$$

where V_{bottom} (L) is the volume of the bottom cell; $i = 1$ represents mussels, $i = 2$ cockles, and $i = 3$ oysters. Based on these filtration rates and shellfish distribution in 2009, *CT* in the western, central, eastern, and northern compartments and the whole basin was 38.7, 18.9, 3.8, 9.0, and 14.6 days, respectively.

To maintain a sustainable aquaculture activity, the filtered external seston should be above the bivalve metabolic needs. We estimated the minimum external POC (particulate organic carbon, in mg L^{-1}) required by bivalves based on their individual *F* and respiration rates *R*. Values of *R* (mg C hr^{-1}) were derived from Bougrier et al. (1995) and Smaal et al. (1997). $R/R_0 = 0.158*(W/W_0)^{0.62}$ for mussels; $R/R_0 = 0.142*(W/W_0)^{0.58}$ for cockles; $R/R_0 = 0.185*(W/W_0)^{0.80}$ for oysters, where $R_0 = 1$ mg C hr^{-1}. Note that all these rates were quantified at 10 °C. In order to calculate POC in the Oosterschelde from the seston data, we multiplied seston concentrations with a POC/seston ratio. We estimated POC in the coastal waters off the Oosterschelde from the Rijkswaterstaat PON (particulate organic nitrogen) data using an observed POC/PON ratio of 8 in this region (Dauby et al., 1994; Huang et al., 2018). The estimated average POC concentration (1.31 mg L^{-1}) is consistent with an earlier study in the southern North Sea (Eisma & Kalf, 1987).

For every grid cell at the end of the simulation, we estimated whether the POC import could balance the POC demand, the latter defined as the amount that meets the respiration needs. The threshold line where imported POC equals the POC demand was mapped spatially for each bivalve species in scenarios with realistic stocks, as well as when halving and doubling the current stocks. In summary, one-year tracer experiments in this study were conducted in four scenarios: no shellfish, and 50%, 100%, and 200% realistic shellfish stocks, and all four scenarios were driven by hydrodynamics simulated for the year 2009.

4. Results

4.1. Model calibration and validation

The modeled water level was compared with observations at four tidal gauges (Figure 1b). During most of the time, the modeled time series of water elevation were in good agreement with observations (e.g., Figure 2). The model skill was further quantified using a Taylor diagram (Figure 3) depicting standard deviations (SDs), correlation coefficients (CCs), and root-mean-square differences (RMSDs) in one graph (Taylor, 2001). Each point in the diagram stands for the comparison of a variable at one location denoted by the calculated SD, CC, and RMSD, and points close to the origins refer to high model skills with low deviations from the measurements and high correlations (Figure 3). Compared to other variables, the model exhibited the best performance for simulated water elevation with all CCs over 0.99 and SDs and RMSDs below 0.1 (Figure 3).

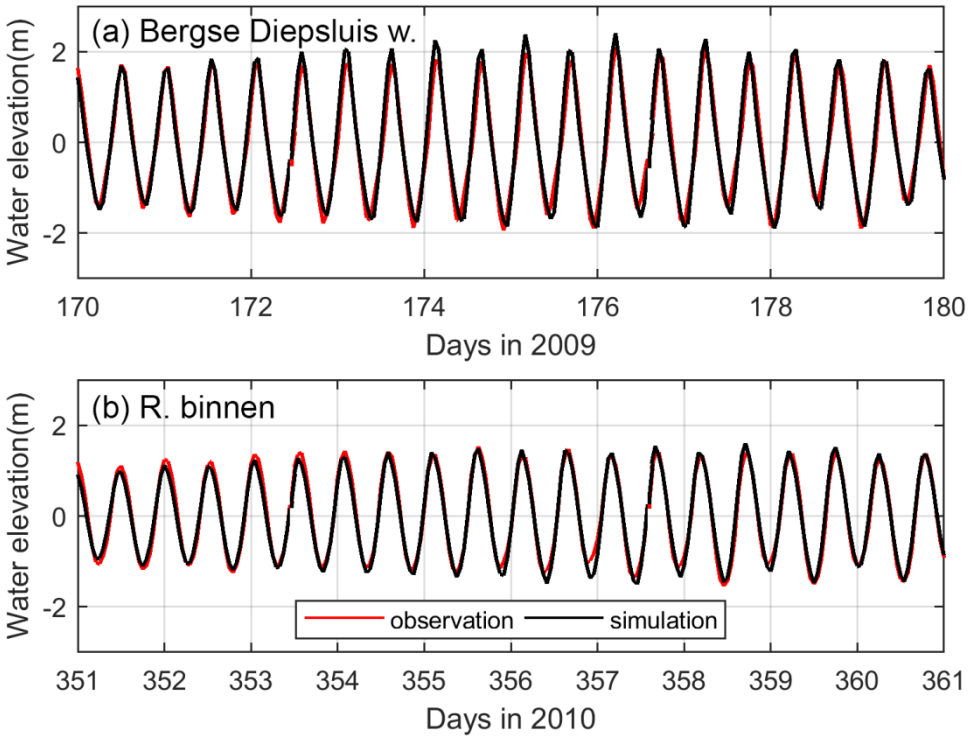

Figure 2. Time series of modeled and observed water elevation at (a) Bergse Diepsluis w. and (b) R. binnen. See Figure 1b for locations of these stations.

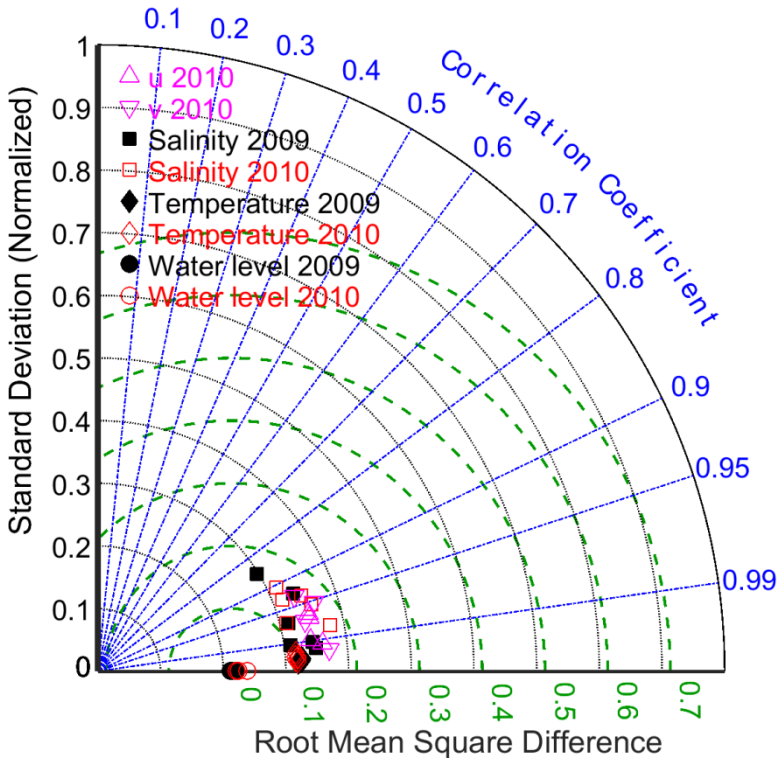

Figure 3. The Taylor diagram of comparisons between model outputs and all available observational data (each point denotes the model-observation comparison at one station). See Figure 1b for all data sites.

To assess the model performance in reproducing the main tidal constituents, harmonic analyses were conducted to the observed and simulated water level data using the code described by Pawlowicz et al. (2002). Tides in the Oosterschelde are dominated by the M2 component; for example, at the station Bergse Diepsluis w., the M2 amplitude (1.48 m) is ~4 times that of the second largest component S2. Figure 4 shows the model accuracy of simulating the main tidal component M2 at four tidal gauges. The simulated errors in the M2 amplitude and phase were within 5% and 10 min, respectively (Figure 4). Note that this falls within the interval at which the data from the tide-gauges is available (viz. at 10-min intervals). The statistical analyses of water level time series and the major tidal component thus reveal excellent skills of the hydrodynamic model.

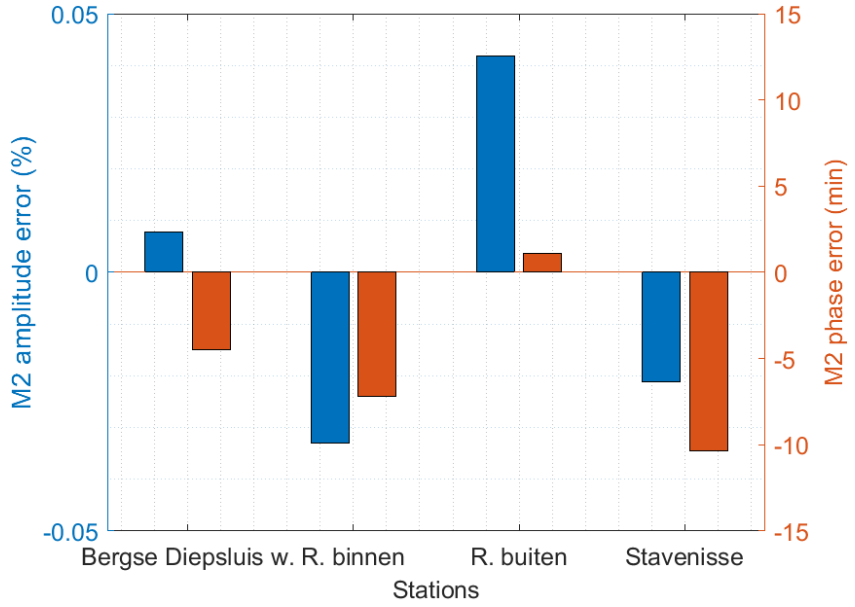

Figure 4. The simulated M2 amplitude and phase errors at four tidal gauges of the Oosterschelde. The amplitude error is relative, calculated as (simulation – observation) / observation. The phase error is absolute, calculated as simulation – observation. See Figure 1b for locations of tidal gauges.

The accuracy of temperature and salinity simulations was also evaluated by comparing them against monthly or biweekly NIOZ shipborne monitoring data. The model captured the main annual cycle of temperature and salinity (e.g., Figure 5). The statistical analyses of all model-data comparisons over the two years indicated CCs of 0.998 ($p < 0.001$) and 0.951 ($p < 0.001$) and RMSD of 0.580 °C and 0.303 for temperature and salinity, respectively ($n = 210$). The temperature model skills for each station clustered closely in the Taylor diagram, while the modeled salinity at one station (7) in 2009 exhibited relatively low correlation (0.85) with the observations (Figure 3). Overall, the model displayed acceptable skills in reproducing realistic temperature and salinity values. This rendered confidence in applying the model in realistic tracer experiments since the advection and dispersion of tracer was computed similarly to those of temperature and salinity (Equation 1).

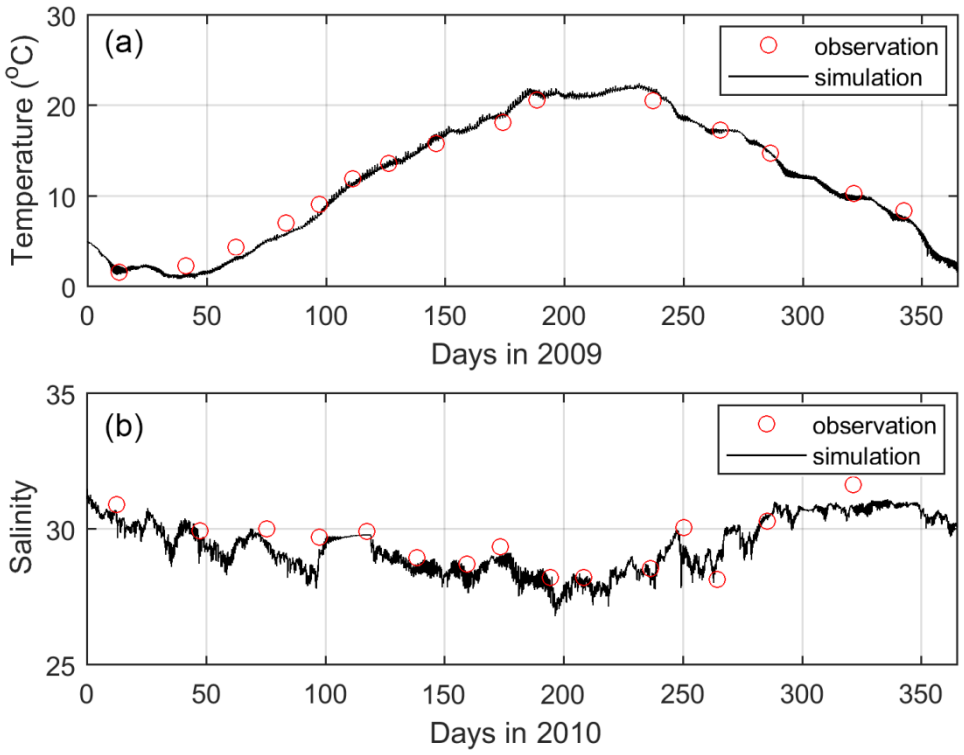

Figure 5. Time series of modeled and observed (a) temperature at Station 3, (b) salinity at Station 7. See Figure 1b for locations of these stations.

Current velocity measured by a ship-mounted ADCP were obtained from the Rijkswaterstaat. The measurements were done within one full tidal cycle (13 h) at different dates and locations around major tidal channels of the Oosterschelde (Figure 1b). Given that the water depth differed among measurements (the measurement location was slightly off sometimes), the depth-average velocity in the model were compared against measurements. Our model was able to capture the phase and maximum magnitude of tidal currents with only minor deviations (e.g., Figure 6). The current measurements were not taken at the exact same spot (the model has a 300 m resolution), which may contribute to the deviations, also considering the steep topography around the main channel (Figure 1b). Overall, the model was robust in simulating tidal currents indicated by the high CCs (0.978 and 0.959 for the eastern and northern components, respectively, $p < 0.001$) and low RMSDs (0.110 m s^{-1} and 0.122 m s^{-1} for the eastern and northern components, respectively, $n = 66$), which ensures the reliability of the tracer transport study with the model. In light of all the above variables, the model skills were well beyond the criteria of reliable estuarine models (Bartlett, 1988).

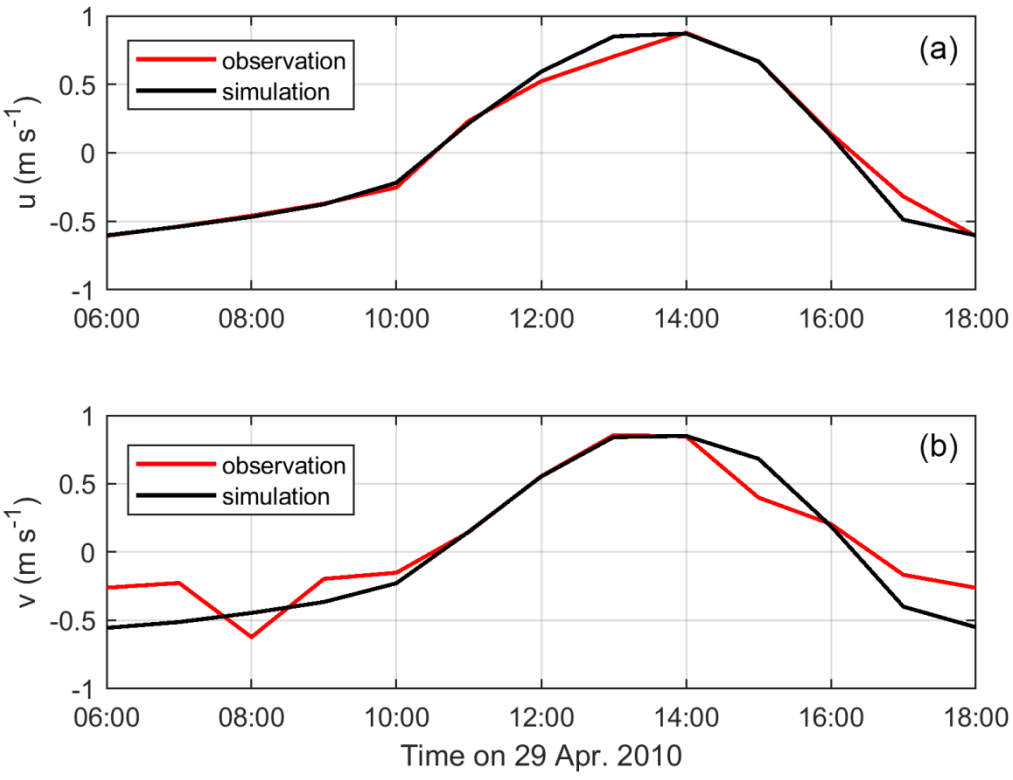

Figure 6. Modeled and observed 13-h depth-average (a) eastward and (b) northward current velocity at 2143R. See Figure 1b for its location.

4.2. Tracer dynamics

With only physical forcing, tracer concentrations in the four compartments reached a plateau after ~250 days and, after 48-h filtering of tide signals, displayed a quasi-exponential increase with time prior to this (Figure 7a). The tracer was replenished fastest in the western compartment and spatial heterogeneity in seston concentration was present most of the time, showing a steady decrease towards the east: western > central > northern > eastern (Figure 7a). The unfiltered tracer concentration showed spring-neap and semi-diurnal tidal variations, the magnitude of which were highest and lowest in the western and northern compartments, respectively (Figure 7a). Both *TT* and *RT*, of similar magnitude (0–150 days) and spatial patterns, revealed the west-east spatial gradient in water renewal (Figure 8). The annual-mean tracer fluxes into the northern and eastern compartments were only 17.1% and 24.4% of that entering the mouth, respectively (Figures 9a). In addition, water renewal timescales were shorter in the south of the western and central compartment and in the north of the eastern compartment (Figures 1 and 8).

If the four compartments were treated as separate systems (the mass change in each compartment was examined with time as Figure 7a), *TT* was 38.3 (western), 88.0 (central), 104.0 (northern), and 116.3 days (eastern), respectively, and the corresponding *RT* was 51.5, 87.5, 105.9, and 111.5 days, respectively. The *CT*/*RT* ratios in these four compartments (0.75, 0.22, 0.03, and 0.09, respectively) are all below one and display a west-east gradient of over-exploitation. These low numbers imply that the seston may be consumed by bivalves faster than replenished by tides, especially in the landward compartments.

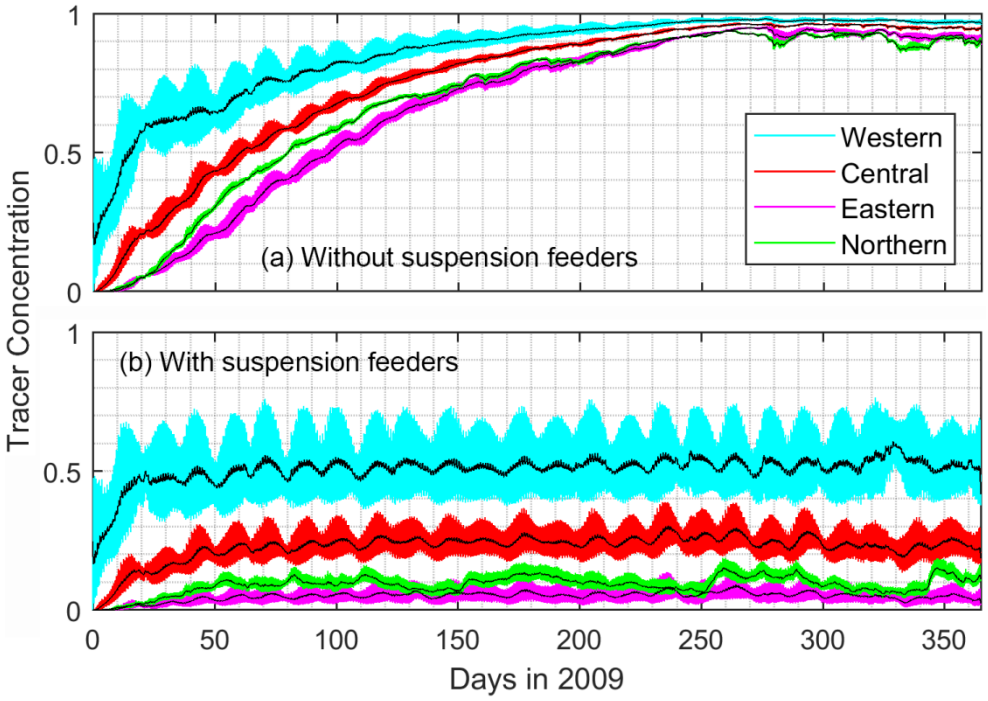

Figure 7. Hourly mean tracer concentrations in four compartments in scenarios (a) without and (b) with suspension feeders for the year 2009. Black lines showed data after 48-h low-pass filtration to remove the daily tidal signals.

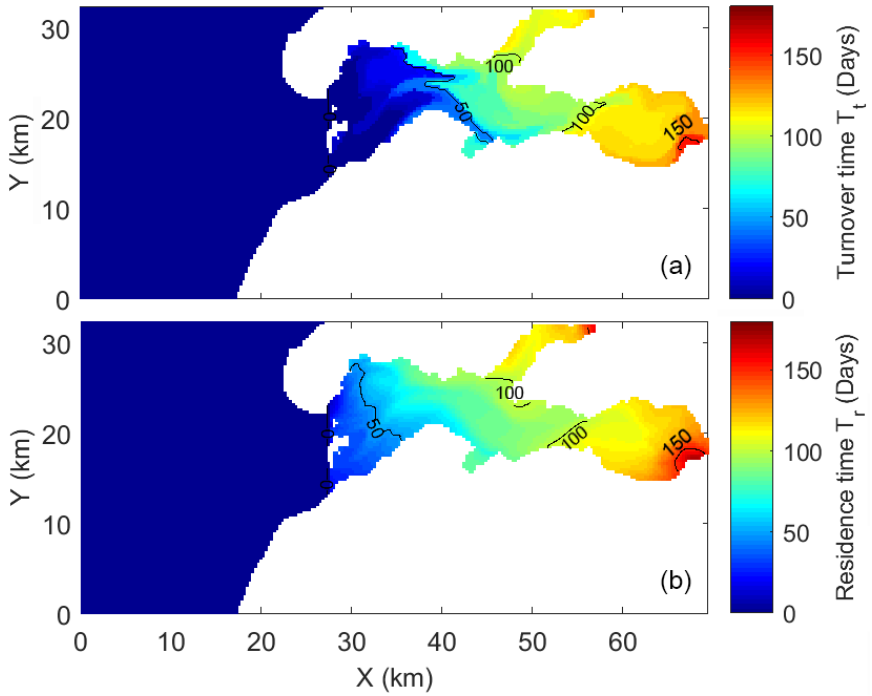

Figure 8. (a) Turnover and (b) residence time in the scenario without suspension feeders estimated in the year 2009.

With the implementation of suspension feeders, tracer influxes into all four compartments were greatly reduced. For instance, the flux into the eastern compartment declined by 79%, and accounted for only 6.2% of that entering the mouth, in contrast to the ratio 24.4% in the physics-only scenario (Figure 9). Tracer renewal and benthic filtration reached the steady state in ~60 days with the equilibrium concentration around 0.5, 0.25, 0.1, and 0.05 for the western, central, northern, and eastern compartments, respectively (Figure 7b). The equilibrium tracer gradient was much stronger between the western and central compartments than between the central and eastern compartments (Figure 10b), which is consistent with the observed patterns in SPM concentrations (Figure 11). Although the tracer/seston herein accounts for a small range (3–100 μm) in the SPM size spectrum, this qualitative phenomenon lends extra weight to our model skill.

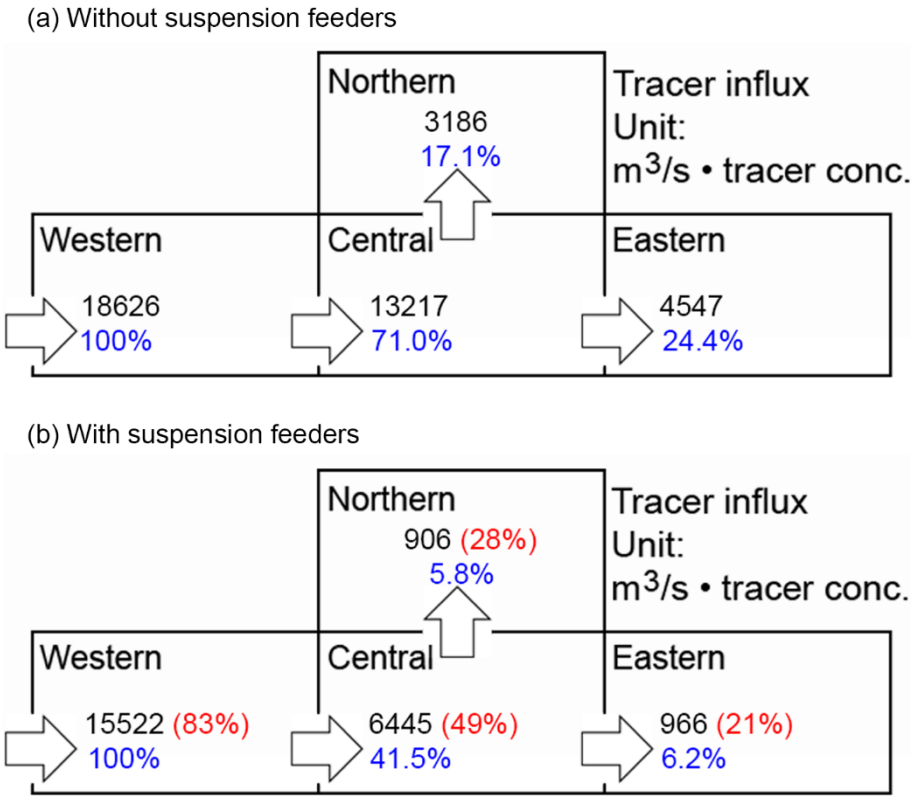

Figure 9. Conceptual diagrams of annually average tracer flux into four compartments in scenarios (a) without and (b) with suspension feeders. Blue numbers are the ratio of tracer fluxes into corresponding compartments to the flux into the bay mouth. Red numbers in brackets in (b) indicate the ratios of influxes in (b) to those in (a) in the same compartment.

Snapshots at the steady state of the tracer concentration (Day 60, 1 March 2009) reveal marked tracer loss in landward (eastern and northern) compartments and shallow regions with large stocks of suspension feeders (e.g., Roggenplaat, Figures 1a, 10a, and 10b). After converting the tracer concentration into POC, the snapshots represent the distribution of imported POC resulting from the balance between tidal import and shellfish consumption (Figure 10). Based on the shellfish physiological rates, the minimum POC concentration that can meet the metabolic needs of these three bivalve species provides a threshold concentration. Below this threshold, shellfish, either wild or cultured, will have to rely on

local production in addition to imported POC. It was found that the equilibrium external seston concentration was below the metabolic needs in 24.6%, 24.9%, and 15.7% of the total area for mussels, cockles, and oysters, respectively, mostly in shallow regions of the central, northern, and eastern compartment (Figure 10b). The threshold lines of mussels and cockles mostly overlapped, while oysters could tolerate a lower POC concentration (Figure 10b). When halving the shellfish stocks, this region was nearly halved and mainly limited to the eastern compartment (Figure 10c). With doubled shellfish biomass, imported POC could not sustain the basic metabolism of mussels, cockles, and oysters in 38.6%, 38.8%, and 29.5% of the Oosterschelde, respectively, comprising the most eastern and northern compartments, and part of the others (Figure 10d).

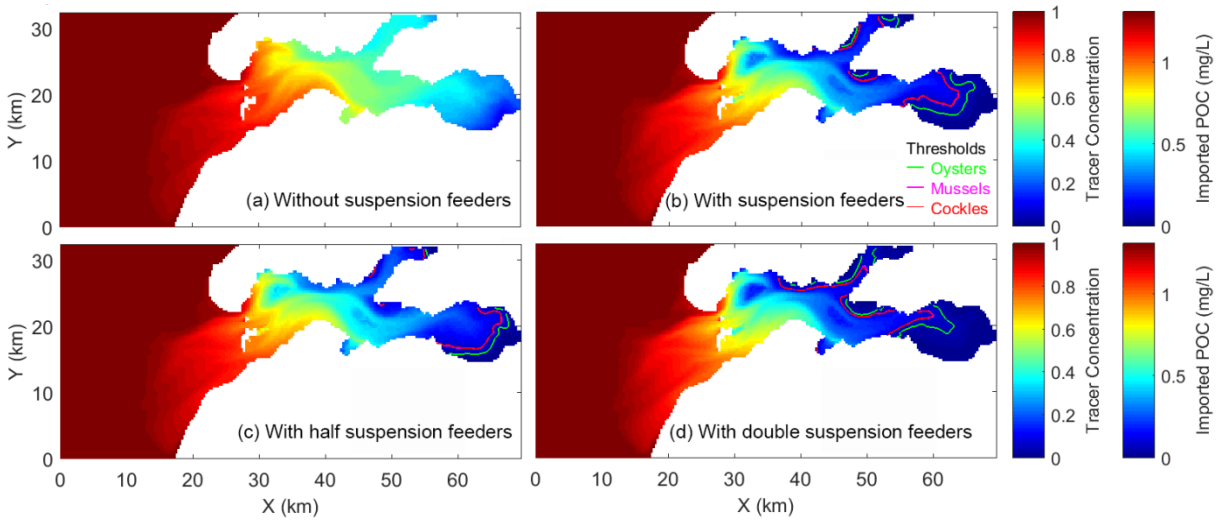

Figure 10. Daily average tracer concentration on 1 March 2009 (when the steady state of the tracer concentration was reached in the scenario with suspension feeders) in the scenarios (a) without suspension feeders, with (b) realistic, (c) half, and (d) double suspension feeders. The threshold lines in (b-d) denote the boundaries where the imported seston can meet the respiration needs of three bivalve species. Due to the similar threshold POC value, the lines for mussels and cockles are mostly overlapped.

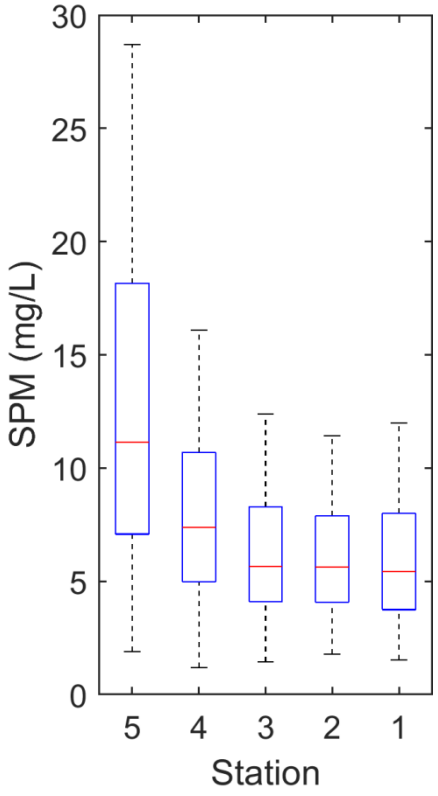

Figure 11. Boxplots of near-surface (~5 m) SPM concentration collected during 1995–2015 at five stations along the main channel of the Oosterschelde. See Figure 1b for locations of these stations.

5. Discussion

With a calibrated and validated hydrodynamic model, this study was set up to demonstrate how physical processes induce significant spatial heterogeneity in tracer replenishment in a tidal bay, the Oosterschelde, and how benthic suspension feeders modify this.

Physical forcing created significant spatial heterogeneity of seston renewal in the Oosterschelde, with both *TT* and *RT* west-east ranges as long as 150 days (Figure 8). There were also other, more subtle gradients. For instance, declining *TT* and *RT* from north to south in the western and central compartments indicated that, of the two main tidal gullies, the southern channel acted as the major conduit of tides (Figures 1 and 8). *TT* and *RT* calculated here (0–150 days) were comparable to the previously reported residence time that was estimated using tidal excursion and total volume (Nienhuis & Smaal, 1994). The renewal time in the Oosterschelde is relatively long compared to many other tidal bays with similar sizes, which can be attributed to the elongated shape, limited freshwater flow, extensive poorly-flushed tidal flats, and the 30% reduction in tidal prism due to the construction of the storm surge barrier (Dame & Prins, 1997; Heip et al., 1995; Nienhuis & Smaal, 1994). Temporal variability of the renewal capability and its response to different physical conditions (e.g., tides, meteorological forcing, gravitational circulation) in the Oosterschelde is not within the scope of this study and will be investigated in the future.

The two proxies for water renewal that are used in this study are based on different rationales. *TT* assumes an exponential decrease of bay water and records the time at which

~63.2% of water is renewed (Zimmerman, 1976). In contrast, *RT* estimates the time to replace the embayment water with external water based on the renewal rate (i.e. how fast the tracer mass changes) in each time step (Takeoka, 1984). Both *TT* and *RT* have been extensively used to depict the spatial variability of the renewal efficiency of estuaries and inshore systems (e.g., Guyondet et al., 2005; Wang et al., 2004; Yuan et al., 2007) and are subject to potential limitations. Deviations from the exponential tracer time series might incur inaccuracy in *TT*; for example, under strong tidal influences, the tracer concentration in the western compartment was not a strict exponential curve (Figure 7a), inducing a relatively large difference (13.2 days) between the two timescales in this region (Figure 8). In contrast, *RT* was computed by integration, and the upper limit of the infinity was replaced by the simulation period (365 days). Thus, due to the cutoff of integration period, underestimates in *RT* are expected, especially in the regions with relatively long *RT*; for example, in the eastern compartment, *RT* was 4.8 days shorter than *TT* (Section 4.2). Despite these biases and limitations, both timescales also displayed similar overall spatial patterns of water renewal in this study (Figure 8). Given the various and sometimes confusing terminology of renewal timescales (Defne & Ganju, 2015; Jouon et al., 2006; Monsen et al., 2002), it is reassured that *TT* and *RT* lead to similar conclusions here.

Resulting tracer concentrations drastically changed after adding realistic stocks of wild and cultured suspension feeders, whose effect was mimicked by model terms representing a bio-deposition force. This removed a large amount of seston already near the mouth (in the western compartment) so that seston flux into the central compartment was reduced by half (Figure 9b). The northern and eastern compartments received even less tracer so that their steady-state concentration was below 10% of that in the North Sea (Figure 7b). This contrasts sharply with the physics-only scenario, where most parts of the Oosterschelde obtained over 90% of the seston concentration in the North Sea given long enough time (Figure 7a). The strong west-east gradient in seston depletion induced by bivalves makes our system an example of comparable biological and physical roles in the system-wide seston budget.

Compared to other systems, such considerable biological impacts depend at least on a large shellfish stock as well as favorable physical conditions that make the most water column available to filter feeders and ensure filtration efficiency (Cranford, 2019; Smaal and van Duren, 2019). With respect to shellfish stocks, the Oosterschelde represents one of the over-exploited coastal bays in the world, as indicated by the high biomass/volume (Figure 12) and low *CT*/*RT* ratio (Figure 23.4 in Smaal and van Duren, 2019). Our results (Figures 7, 9, and 10) indicate a strong gradient in seston depletion in such systems, in contrast to those with limited or depleted shellfish stocks such as Chesapeake and Delaware Bays (Ashton-Alcox et al., 2018; Jordan et al., 2002).

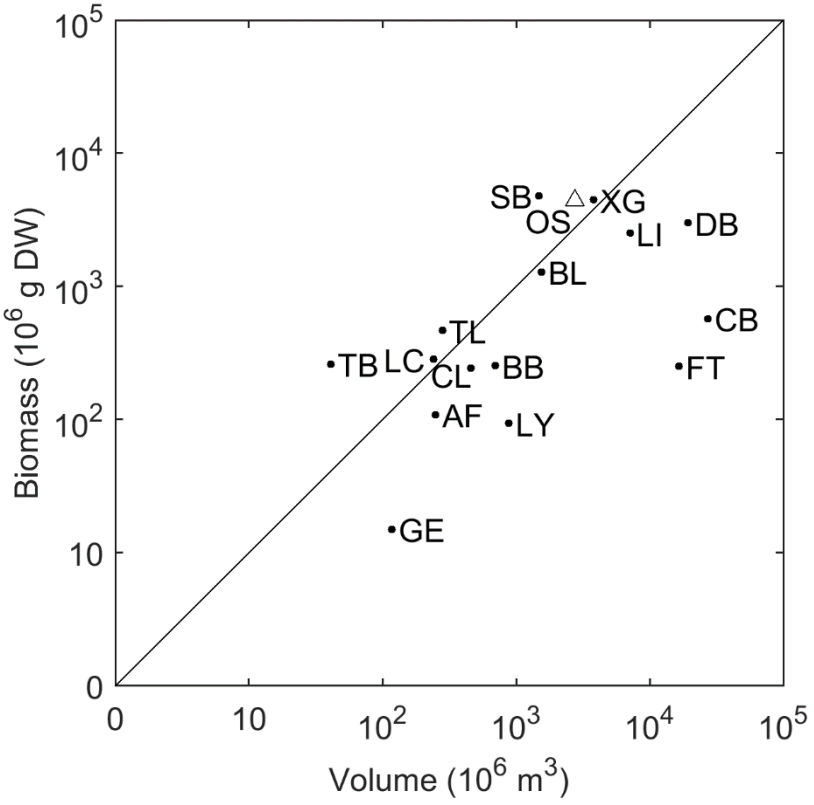

458

459 **Figure 12.** Scatter plots of shellfish biomass in dry weight against the system volume in 16
460 nearshore estuaries or coastal bays. The Oosterschelde is marked with an open triangle and
461 other systems with dots. The abbreviations and data references are OS (the Oosterschelde);
462 AF (Åfjord, Norway), BL (Belfast Lough, UK), LI (Limfjorden, Denmark), LY (Lysefjord,
463 Norway) (Jansen et al., 2019); BB (Beatrix Bay, New Zealand, Gibbs, 2007); CL (Carlingford
464 Lough, UK), GE (Grande-Entrée Lagoon, Canada), LC (Loch Creran, UK), SB (Sanggou
465 Bay, China), XG (Xiangshan Gang, China) (Smaal & van Duren, 2019); CB (Chesapeake
466 Bay, US, Jordan et al., 2002); DB (Delaware Bay, US, Ashton-Alcox et al., 2018); FT (Firth
467 of Thames, New Zealand, Zeldis, 2005); TL (Thau Lagoon, France, Gangnery et al., 2011);
468 TB (Tracadie Bay, Canada, Cranford et al., 2007), respectively.

469 Besides shellfish biomass, physical conditions that frequently replenish near-bed
470 waters and minimize refiltration of the prefiltered water are also essential for strong bivalve-
471 induced seston removal. We estimated the refiltration ratio by comparing the bulk and
472 realistic clearance rates. As an indicator of systemwide filtration capacity, the bulk *CT* is
473 derived by dividing the water volume by the filtration rate (Dame & Prins, 1997), which,
474 however, overlooks refiltration and overestimates the seston removal rate (Boegman et al.,
475 2008; Cranford, 2019). In contrast, the *CT* calculated in our model accounts for refiltration by
476 considering advection and dispersion of filtered water masses. The bulk clearance rate in the
477 Oosterschelde is 0.068 day^{-1} (bulk *CT* = 14.6 days), while the model-computed clearance rate
478 is 0.051 day^{-1}, suggesting refiltration of approximately one third of the basin volume. This
479 refiltration ratio is relatively low compared to some stagnant or stratified systems (Cranford,
480 2019; O'riordan et al., 1995; Yu & Culver, 1999), given that the Oosterschelde is well-mixed
481 and that most culture plots are located in shallow regions rather than channels (Figure 1a).

482 Despite the strong filtration pressure, our findings demonstrate that the imported
483 seston alone can meet the basic metabolic needs of shellfish stocks in 75%–85% of the bay

area in 2009 (Figure 10b), which contrasts with studies suggesting that the grazing pressure is so high that *in situ* primary production cannot meet the food demand of current bivalve populations during this period (Smaal et al., 2013). The sites where food import is beyond the shellfish metabolic demands are mostly in the eastern and northern compartments where extremely low CT/RT ratios (<0.1) demonstrate unsustainable overexploitation but most oyster plots and wild cockle populations are located (Figures 1b and 10b). These results suggest that these organisms do rely on local primary production, which, in this area, can be stimulated by regenerated nutrients on the shellfish bed (Prins & Smaal, 1994).

Our study offers a promising methodology of assessing food conditions for ecosystems with important aquaculture activities that rely mostly on marine import (e.g., Spillman et al., 2008). Firstly, the system-wide mapping of seston renewal efficiency allows designating areas that are more suitable for aquaculture and to test the consequences that farming activities have for food conditions of the total area. Secondly, by mapping the area where imported food is sufficient to sustain bivalve physiological demands (Figure 10), the potential dependence on external versus local food sources is demonstrated. The fraction of this area compared to the total area is also an easily extractable and interpretable measure that allows comparing various aquaculture-dominated bays similar to the Oosterschelde. Our modeling approach is simple and considers only mass changes of a non-decaying tracer driven by a hydrodynamic model and modified by uptake of filter feeders, whose density and distribution are imposed. For an area where the bivalve populations are predominantly under human control (Smaal et al., 2013), imposing measured impacts of filter feeders is to be preferred over complicated pelagic and benthic ecological models that include a lot more assumptions, parameterizations, uncertainties, and computational burden (Nunes et al., 2011; Scavia et al., 2006).

However, it is noteworthy that our model is not a dynamic sediment transport model. The resuspension, settling, and wave-induced motion are not represented in our seston simulation, and thus the modeled tracer cannot fully account for the spatiotemporal SPM dynamics (e.g., Figure 11). Moreover, our grid size (300 m × 300 m) is about the same as a commercial culture plot and is insufficient to pinpoint the optimal location and project the yield for specific culture plots. In regions with complicated topography (e.g, steep channel flanks), coarse-resolution models may induce numerical inaccuracy in simulating transport processes due to lacking bathymetry details (e.g., Jiang and Xia, 2016). Thereby, for site-specific biophysical studies or sediment transport or geomorphological models, a refined spatial (horizontal and vertical) resolution is needed.

6. Conclusions

A three-dimensional hydrodynamic model (GETM) was applied, calibrated, and validated for the Oosterschelde to investigate seston renewal from the North Sea. The tracer experiment driven with physical forcing revealed a large west-east gradient in seston renewal time. Given sufficient time (~250 days), seston in most areas reached over 90% of the concentration in the North Sea. When filter feeders were implemented, the strong benthic bio-deposition reduced the seston influxes and steady-state concentrations in all parts of the system, especially in the landward compartments. This shows that that biological influences on seston can be as important if not more important than physical forcing in ecosystems with substantial aquaculture activities. The gradient in seston depletion induced by biophysical factors should be fully considered in tidal bays that are intensively used for aquaculture.

Acknowledgments

This work was supported by the collaborative framework of Utrecht University and NIOZ and by the INNOPRO project which was funded by the European Union through the European Maritime and Fisheries Fund (EMFF) and the Producers' Organization of the Dutch mussel culture (POM). We thank Johan van der Molen (NIOZ) for providing the open boundary conditions, Raymond Sluiter (KNMI) and Henk van den Brink (KNMI) for information on the meteorological data, and Marco Schrijver (Rijkswaterstaat) and Jan van 't Westende (Rijkswaterstaat) for sharing the velocity measurements. Research data can be accessed on the repository https://github.com/ljiang2/os_sf.

References

Ashton-Alcox, K. A., Bushek, D., & Morson, J. (2018). Stock assessment workshop New Jersey Delaware Bay oyster beds (20th SAW). Rutgers New Jersey Agricultural Experiment Station: Haskin Shellfish Research Laboratory.

Aubrey, D. G., McSherry, T. R., & Eliet, P. P. (1993). Effects of multiple inlet morphology on tidal exchange: Waquoit Bay, Massachusetts. *Formation and Evolution of Multiple Tidal Inlets*, 213–235.

Bartlett, J. M. (1998), Quality control manual for computational estuarine modelling, *R&D Tech. Rep. WI 68*, Environ. Agency, Almondsbury, U. K.

Boegman, L., Loewen, M. R., Hamblin, P. F., & Culver, D. A. (2008). Vertical mixing and weak stratification over zebra mussel colonies in western Lake Erie. *Limnology and Oceanography*, 53(3), 1093–1110.

Bougrier, S., Geairon, P., Deslous-Paoli, J. M., Bacher, C., & Jonquières, G. (1995). Allometric relationships and effects of temperature on clearance and oxygen consumption rates of *Crassostrea gigas* (Thunberg). *Aquaculture*, 134(1–2), 143–154.

Boynton, W. R., Garber, J. H., Summers, R., & Kemp, W.M. (1995). Inputs, transformations, and transport of nitrogen and phosphorus in Chesapeake Bay and selected tributaries. *Estuaries*, 18, 285–314.

Burchard, H., Bolding, K., & Villarreal, M. R. (2004). Three-dimensional modelling of estuarine turbidity maxima in a tidal estuary. *Ocean Dynamics*, 54(2), 250–265.

Carter, L. (1976). Seston transport and deposition in Pelorus sound, South Island, New Zealand. *New Zealand Journal of Marine and Freshwater Research*, 10(2), 263–282.

Chaparro, O. R., Segura, C. J., Montiel, Y. A., Thompson, R. J., & Navarro, J. M. (2008). Variations in the quantity and composition of seston from an estuary in southern Chile on different temporal scales. *Estuarine, Coastal and Shelf Science*, 76(4), 845–860.

Coosen, J., Twisk, F., van der Tol, M. W. M., Lambeck, R. H. D., van Stralen, M. R., & Meire, P. M. (1994). Variability in stock assessment of cockles (*Cerastoderma edule* L.) in the Oosterschelde (in 1980–1990), in relation to environmental factors. *Hydrobiologia*, 282/283, 381–395.

Cranford, P. J. (2019). Magnitude and extent of water clarification services provided by bivalve suspension feeding. In Goods and Services of Marine Bivalves. Springer.

Cranford, P. J., Strain, P. M., Dowd, M., Hargrave, B. T., Grant, J., & Archambault, M. C. (2007). Influence of mussel aquaculture on nitrogen dynamics in a nutrient enriched coastal embayment. *Marine Ecology Progress Series*, 347, 61–78.

572 Cranford, P. J., Ward, J. E., & Shumway, S. E. (2011). Bivalve filter feeding: variability and
573 limits of the aquaculture biofilter. In *Shellfish Aquaculture and the Environment* (pp.
574 179–188), Wiley-Blackwell.

575 Dame, R. F., & Prins, T. C. (1997). Bivalve carrying capacity in coastal ecosystems. *Aquatic*
576 *Ecology*, 31(4), 409–421.

577 Dauby, P., Frankignoulle, M., Gobert, S., & Bouquegneau, J. M. (1994). Distribution of POC,
578 PON, and particulate Al, Cd, Cr, Cu, Pb, Ti, Zn and $\delta^{13}C$ in the English-channel and
579 adjacent areas. *Oceanologica Acta*, 17(6), 643–657.

580 Defne, Z., & Ganju, N. K. (2015). Quantifying the residence time and flushing characteristics
581 of a shallow, back-barrier estuary: Application of hydrodynamic and particle tracking
582 models. *Estuaries and Coasts*, 38(5), 1719–1734.

583 Duran-Matute, M., Gerkema, T., De Boer, G. J., Nauw, J. J., & Gräwe, U. (2014). Residual
584 circulation and freshwater transport in the Dutch Wadden Sea: a numerical modelling
585 study. *Ocean Science*, 10(4), 611–632.

586 Egbert, G. D., Erofeeva, S. Y., & Ray, R. D. (2010). Assimilation of altimetry data for
587 nonlinear shallow-water tides: Quarter-diurnal tides of the Northwest European Shelf.
588 *Continental Shelf Research*, 30(6), 668–679.

589 Eisma, D., & Kalf, J. (1987). Distribution, organic content and particle size of suspended
590 matter in the North Sea. *Netherlands Journal of Sea Research*, 21(4), 265–285.

591 Filgueira, R., Comeau, L. A., Guyondet, T., McKindsey, C. W., & Byron, C. J. (2015).
592 Modelling carrying capacity of bivalve aquaculture: a review of definitions and
593 methods. In *Encyclopedia of Sustainability Science and Technology*. Springer, New
594 York.

595 Filgueira, R., Guyondet, T., Comeau, L. A., & Grant, J. (2014). A fully-spatial ecosystem-
596 DEB model of oyster (*Crassostrea virginica*) carrying capacity in the Richibucto
597 Estuary, Eastern Canada. *Journal of Marine Systems*, 136, 42–54.

598 Flagg, C. N., Vermersch, J. A., & Beardsley, R. C. (1974). MIT New England Shelf
599 Dynamics Experiment (March, 1974) Data Report, Part II: The moored array. MIT
600 Rep, 76(1), 531–546.

601 Gangnery, A., Bacher, C., & Buestel, D. (2001). Assessing the production and the impact of
602 cultivated oysters in the Thau lagoon (Mediterranee, France) with a population
603 dynamics model. *Canadian Journal of Fisheries and Aquatic Sciences*, 58(5), 1012–
604 1020.

605 Gibbs, M. T. (2007). Sustainability performance indicators for suspended bivalve aquaculture
606 activities. *Ecological Indicators*, 7(1), 94–107.

607 Grangeré, K., Lefebvre, S., Bacher, C., Cugier, P., & Ménesguen, A. (2010). Modelling the
608 spatial heterogeneity of ecological processes in an intertidal estuarine bay: dynamic
609 interactions between bivalves and phytoplankton. *Marine Ecology Progress Series*,
610 415, 141–158.

611 Grant, J., & Filgueira, R. (2011). The application of dynamic modeling to prediction of
612 production carrying capacity in shellfish farming. *Shellfish aquaculture and the*
613 *environment*, 135–154.

614 Guyondet, T., Comeau, L. A., Bacher, C., Grant, J., Rosland, R., Sonier, R., & Filgueira, R.
615 (2015). Climate change influences carrying capacity in a coastal embayment dedicated
616 to shellfish aquaculture. *Estuaries and Coasts*, 38(5), 1593–1618.

617 Guyondet, T., Koutitonsky, V. G., & Roy, S. (2005). Effects of water renewal estimates on
618 the oyster aquaculture potential of an inshore area. *Journal of Marine Systems*, 58, 35–
619 51.

620 Guyondet, T., Sonier, R., & Comeau, L. A. (2013). Spatially explicit seston depletion index to
621 optimize shellfish culture. *Aquaculture Environment Interactions*, 4(2), 175–186.

622 Heip, C. H. R., Goosen, N. K., Herman, P. M. J., Kromkamp, J. C., Middelburg, J. J., &
623 Soetaert, K. E. R. (1995). Production and consumption of biological particles in
624 temperate tidal estuaries. *Oceanography and Marine Biology: An annual review*, 33,
625 1–149.

626 Huang, C., Jiang, Q., Yao, L., Yang, H., Lin, C., Huang, T., Zhu, A-X., & Zhang, Y. (2018).
627 Variation pattern of particulate organic carbon and nitrogen in oceans and inland
628 waters. *Biogeosciences*, 15(6), 1827–1841.

629 Jansen, H. M., Strand, Ø., van Broekhoven, W., Strohmeier, T., Verdegem, M. C., & Smaal,
630 A. C. (2019). Feedbacks from filter feeders: review on the role of mussels in cycling
631 and storage of nutrients in oligo-meso-and eutrophic cultivation areas. In *Goods and*
632 *Services of Marine Bivalves*, edited by Smaal et al., Springer, Cham, Switzerland.

633 Jiang, L., & Xia, M. (2016). Dynamics of the Chesapeake Bay outflow plume: Realistic
634 plume simulation and its seasonal and interannual variability. *Journal of Geophysical*
635 *Research: Oceans*, 121(2), 1424–1445.

636 Jordan, S. J., Greenhawk, K. N., McCollough, C. B., Vanisko, J., & Homer, M. L. (2002).
637 Oyster biomass, abundance, and harvest in northern Chesapeake Bay: trends and
638 forecasts. *Journal of Shellfish Research*, 21(2), 733–742.

639 Jouon, A., Douillet, P., Ouillon, S., & Fraunié, P. (2006). Calculations of hydrodynamic time
640 parameters in a semi-opened coastal zone using a 3D hydrodynamic model.
641 *Continental Shelf Research*, 26, 1395–1415.

642 Koutitonsky, V. G., Guyondet, T., St-Hilaire, A., Courtenay, S. C., & Bohgen, A. (2004).
643 Water renewal estimates for aquaculture developments in the Richibucto estuary,
644 Canada. *Estuaries*, 27(5), 839–850.

645 Luff, R., & Pohlmann, T. (1995). Calculation of water exchange times in the ICES-boxes with
646 a eulerian dispersion model using a half-life time approach. *Deutsche Hydrografische*
647 *Zeitschrift*, 47(4), 287–299.

648 Mohrholz, V., Naumann, M., Nausch, G., Krüger, S., & Gräwe, U. (2015). Fresh oxygen for
649 the Baltic Sea—An exceptional saline inflow after a decade of stagnation. *Journal of*
650 *Marine Systems*, 148, 152–166.

651 Monsen, N. E., Cloern, J. E., Lucas, L. V., & Monismith, S. G. (2002). A comment on the use
652 of flushing time, residence time, and age as transport time scales. *Limnology and*
653 *oceanography*, 47(5), 1545–1553.

654 Moser, G. A., Gianesella, S. M. F., Alba, J. J. B., Bérgamo, A. L., Saldanha-Corrêa, F. M.,
655 Miranda, L. B. D., & Harari, J. (2005). Instantaneous transport of salt, nutrients,
656 suspended matter and chlorophyll-a in the tropical estuarine system of Santos.
657 *Brazilian Journal of Oceanography*, 53(3–4), 115–127.

Nienhuis, P. H., & Smaal, A. C. (1994). The Oosterschelde estuary, a case-study of a changing ecosystem: an introduction. *Hydrobiologia*, 282/283, 1–14.

Nunes, J. P., Ferreira, J. G., Bricker, S. B., O'Loan, B., Dabrowski, T., Dallaghan, B., ... & O'Carroll, T. (2011). Towards an ecosystem approach to aquaculture: Assessment of sustainable shellfish cultivation at different scales of space, time and complexity. *Aquaculture*, 315(3–4), 369–383.

O'riordan, C. A., Monismith, S. G., & Koseff, J. R. (1995). The effect of bivalve excurrent jet dynamics on mass transfer in a benthic boundary layer. *Limnology and Oceanography*, 40(2), 330-344.

Pawlowicz, R., Beardsley, B., & Lentz, S. (2002). Classical tidal harmonic analysis including error estimates in MATLAB using T_TIDE. Computers & Geosciences, 28(8), 929–937.

Prins, T. C., & Smaal, A. C. (1994). The role of the blue mussel *Mytilus edulis* in the cycling of nutrients in the Oosterschelde estuary (The Netherlands). *Hydrobiologia*, 282/283, 413–429.

North, E. W., Chao, S. Y., Sanford, L. P., & Hood, R. R. (2004). The influence of wind and river pulses on an estuarine turbidity maximum: Numerical studies and field observations in Chesapeake Bay. *Estuaries*, 27(1), 132–146.

Prins, T. C., Smaal, A. C., Pouwer, A. J., & Dankers, N. (1996). Filtration and resuspension of particulate matter and phytoplankton on an intertidal mussel bed in the Oosterschelde estuary (SW Netherlands). *Marine Ecology Progress Series*, 121–134.

Scavia, D., Kelly, E. L., & Hagy, J. D. (2006). A simple model for forecasting the effects of nitrogen loads on Chesapeake Bay hypoxia. *Estuaries and Coasts*, 29(4), 674–684.

Shen, J., & Wang, H. V. (2007). Determining the age of water and long-term transport timescale of the Chesapeake Bay. *Estuarine, Coastal and Shelf Science*, 74(4), 585–598.

Smaal, A. C., Kater, B. J., & Wijsman, J. W. M. (2009). Introduction, establishment and expansion of the Pacific oyster *Crassostrea gigas* in the Oosterschelde (SW Netherlands). *Helgoland Marine Research*, 63(1), 75.

Smaal, A. C., Schellekens, T., van Stralen, M. R., & Kromkamp, J. C. (2013). Decrease of the carrying capacity of the Oosterschelde estuary (SW Delta, NL) for bivalve filter feeders due to overgrazing?. *Aquaculture*, 404, 28–34.

Smaal, A. C., & van Duren, L. A. (2019). Bivalve aquaculture carrying capacity: concepts and assessment tools. In *Goods and Services of Marine Bivalves*, edited by Smaal et al., Springer, Cham, Switzerland.

Smaal, A. C., & van Stralen, M. R. (1990). Average annual growth and condition of mussels as a function of food source. In *North Sea—Estuaries Interactions* (pp. 179–188). Springer, Dordrecht.

Smaal, A., van Stralen, M. R., & Schuiling, E. (2001). The interaction between shellfish culture and ecosystem processes. *Canadian Journal of Fisheries and Aquatic Sciences*, 58(5), 991–1002.

Smaal, A. C., Vonck, A. P. M. A., & Bakker, M. (1997). Seasonal variation in physiological energetics of *Mytilus edulis* and *Cerastoderma edule* of different size classes. *Journal of the Marine Biological Association of the United Kingdom*, 77(3), 817–838.

Spillman, C. M., Hamilton, D. P., Hipsey, M. R., & Imberger, J. (2008). A spatially resolved model of seasonal variations in phytoplankton and clam (*Tapes philippinarum*) biomass in Barbamarco Lagoon, Italy. *Estuarine, Coastal and Shelf Science*, 79(2), 187–203.

Takeoka, H. (1984). Fundamental concepts of exchange and transport time scales in a coastal sea. *Continental Shelf Research*, 3(3), 311–326.

Tangelder, M., Troost, K., van den Ende, D., & Ysebaert, T. (2012). *Biodiversity in a changing Oosterschelde: from past to present*. Wettelijke Onderzoekstaken Natuur & Milieu, WOT work document 288, 52p.

Taylor, K. E. (2001). Summarizing multiple aspects of model performance in a single diagram. *Journal of Geophysical Research*, 106(D7), 7183–7192.

van der Molen, J., Ruardij, P., & Greenwood, N. (2016). Potential environmental impact of tidal energy extraction in the Pentland Firth at large spatial scales: results of a biogeochemical model. *Biogeosciences*, 13, 2593–2609.

van Stralen, M. R., & Dijkema, R. D. (1994). Mussel culture in a changing environment: the effects of a coastal engineering project on mussel culture (*Mytilus edulis* L.) in the Oosterschelde estuary (SW Netherlands). *Hydrobiologia*, 282/283, 359–379.

Wang, C. F., Hsu, M. H., & Kuo, A. Y. (2004). Residence time of the Danshuei River estuary, Taiwan. Estuarine, Coastal and Shelf Science, 60(3), 381–393.

Wetsteyn, L. P. M. J., & Kromkamp, J. C. (1994). Turbidity, nutrients and phytoplankton primary production in the Oosterschelde (The Netherlands) before, during and after a large-scale coastal engineering project (1980–1990). *Hydrobiologia*, 282/283, 61–78.

Wijsman, J. W. M., & Smaal, A. C. (2017). The use of shellfish for pre-filtration of marine intake water in a reverse electro dialysis energy plant; Inventory of potential shellfish species and design of conceptual filtration system. *Report C078/17*, Wageningen Marine Research, the Netherlands.

Wijsman, J. W. M., Troost, K., Fang, J., and Roncarati, A. (2019). Global production of marine bivalves: Trends and challenges. In *Goods and Services of Marine Bivalves*, edited by Smaal et al., Springer, Cham, Switzerland.

Wildish, D. J., & Kristmanson, D. D. (1993). Hydrodynamic control of bivalve filter feeders: a conceptual view. In *Bivalve Filter Feeders* (pp. 299–324). Edited by R. F. Dame. Springer, Berlin, Heidelberg.

Ysebaert, T., van der Hoek, D. J., Wortelboer, R., Wijsman, J. W. M., Tangelder, M., & Nolte, A. (2016). Management options for restoring estuarine dynamics and implications for ecosystems: A quantitative approach for the Southwest Delta in the Netherlands. *Ocean & Coastal Management*, 121, 33–48.

Yu, N., & Culver, D. A. (1999). Estimating the effective clearance rate and refiltration by zebra mussels, *Dreissena polymorpha*, in a stratified reservoir. *Freshwater Biology*, 41(3), 481-492.

Yuan, D., Lin, B., & Falconer, R. A. (2007). A modelling study of residence time in a macro-tidal estuary. Estuarine, Coastal and Shelf Science, 71, 401–411.

Zeldis, J. (2005). Magnitudes of natural and mussel farm-derived fluxes of carbon and nitrogen in the Firth of Thames. NIWA client report: CHC2005–048.

745 Zimmerman, J. T. F. (1976). Mixing and flushing of tidal embayments in the western Dutch
746 Wadden Sea part I: Distribution of salinity and calculation of mixing time scales.
747 *Netherlands Journal of Sea Research*, 10(2), 149–191.